

# Condensation heat transfer and pressure drop of R-410A in flat aluminum multi-port tubes

Nae-Hyun Kim<sup>1</sup>

Received: 30 March 2017 / Accepted: 31 August 2017 / Published online: 12 September 2017  
© Springer-Verlag GmbH Germany 2017

**Abstract** Brazed heat exchangers with aluminum flat multi-port tubes are being used as condensers of residential air-conditioners. In this study, R-410A condensation tests were conducted in four multi-port tubes having a range of hydraulic diameter ( $0.78 \leq D_h \leq 0.95$  mm). The test range covered the mass flux from 100 to 400 kg/m<sup>2</sup>s and the heat flux at 3 kW/m<sup>2</sup>, which are typical operating conditions of residential air conditioners. Results showed that both the heat transfer coefficient and the pressure drop increased as the hydraulic diameter decreased. The effect of hydraulic diameter on condensation heat transfer was much larger than the predictions of existing correlations for the range of investigation. Comparison of the data with the correlations showed that some macro-channel tube correlations and mini-channel tube correlations reasonably predicted the heat transfer coefficient. However, macro-channel correlations highly overpredicted the pressure drop data.

## Nomenclature

$A$	heat transfer area, mm <sup>2</sup>
$A_c$	cross-sectional flow area, mm <sup>2</sup>
$A_i$	total internal surface area, mm <sup>2</sup>
$b$	thickness of the flat tube, mm
$c_p$	specific heat, J/kg K
$D_h$	hydraulic diameter, mm
$G$	mass flux, kg/m <sup>2</sup> s
$h$	heat transfer coefficient, W/m <sup>2</sup> K
$i_{fg}$	latent heat of vaporization, J/kg

$k$	thermal conductivity, W/mK
$L$	length of the test section, mm
$m$	mass flow rate, kg/s
$N$	number of ports in a multi-port tube
$P$	pressure, N/m <sup>2</sup>
$P_w$	wetted perimeter, mm
$q$	heat flux, W/m <sup>2</sup>
$Q$	heat transfer rate, W
$R$	variable
$T$	temperature, K
$t$	tube wall thickness, mm
$U$	overall heat transfer coefficient, W/m <sup>2</sup> K
$v$	specific volume, m <sup>3</sup> /kg
$w$	width of the flat tube, mm or uncertainty of the variable
$x$	vapor quality or measured variable
$z$	coordinate parallel to the flow, mm

## Subscripts

a	acceleration
ave	average
corr	correlation
exp	experimental
i	tube-side
in	inlet
f	liquid, friction
g	gas, gravitation
lm	log mean
m	mean
o	annular-side
out	outlet
p	pre-heater
pred	predicted
r	refrigerant
sat	saturation
w	water

✉ Nae-Hyun Kim  
knh0001@inu.ac.kr

<sup>1</sup> Department of Mechanical Engineering, Incheon National University, 12-1, Songdo-Dong, Yeonsu-Gu, Incheon 406-772, Republic of Korea

## 1 Introduction

Fin-and-round tube heat exchangers have long been used as condensers in an air-conditioning system, and rigorous efforts have been made to improve the thermal performance of the heat exchangers. These include a usage of high performance fins, and of small diameter tubes, etc. However, fin-and-round tube heat exchangers have inherent short-comings such as contact resistance between fins and tubes, existence of low performance region behind tubes, etc. These short-comings may be mitigated if low-profile flat tubes are used, fins and tubes are soldered [1]. Brazed heat exchangers with aluminum louver fins and aluminum flat multi-port tubes satisfy the requirements, and have long been used as condensers of automotive air-conditioning units, and are being used as condensers of residential air-conditioners. For a proper design of the brazed aluminum heat exchanger, knowledge on condensation heat transfer and pressure drop characteristics in the flat multi-port tube is mandatory.

The literature shows fair amount of studies on condensation heat transfer and pressure drop in multi-port tubes. Existing studies are summarized in Table 1. Yang and Webb [2] and Webb and Yang [3] conducted condensation heat transfer tests using R-12 and R-134a in smooth ( $D_h = 2.64$  mm) or micro-

finned ( $D_h = 1.56$  mm) multi-port tubes, both having 4 channels. The test range covered  $400 \leq G \leq 1400$  kg/m<sup>2</sup> s,  $4 \leq q \leq 12$  kW/m<sup>2</sup> at  $T_{\text{sat}} = 65$  °C. They showed that the data were reasonably predicted by Akers et al. [21] correlation. The data were underpredicted by Shah [22] correlation. The heat transfer coefficients of the micro-finned tube were 10 to 60% higher than those of the smooth tube for the entire test range. The difference increased as vapor quality increased. They attributed the trend to the additional surface-tension drainage condensation on the fin surface, which is exposed to vapor at high vapor quality. Yang and Webb [4] reported pressure drop data for the same tubes tested by Yang and Webb [22]. The pressure drop of the micro-finned tube was higher than that of the smooth tube. They successfully correlated the pressure drop data using the equivalent mass velocity concept proposed by Akers et al. [21]. A semi-empirical model that accounts for the vapor shear and surface tension to predict the condensation heat transfer for micro-finned multiport tubes was proposed by Yang and Webb [23].

Chang et al. [5] tested four multi-port tubes (two smooth and two micro-finned) having 5 to 7 channels using R-22 ( $T_{\text{sat}} = 45$  °C) and R-134a ( $T_{\text{sat}} = 40$  °C). Their mass flux range, however, was rather low ( $30 \leq G \leq 100$  kg/m<sup>2</sup> s). Microfin tubes yielded 10 to 15% higher condensation heat transfer coefficients than smooth tubes for the entire test range. Wang et al. [6] tested

**Table 1** Previous studies on condensation in multi-port flat tubes

Authors	Tube shape	$D_h$ (mm)	n	Refrigerant	G (kg/m <sup>2</sup> s)	$T_{\text{sat}}$ (°C)	q (kW/m <sup>2</sup> )
Yang and Webb [2–4]	smooth-rec micro-rec	2.64 1.56	4 4	R-12 R-134a	400–1000	65	4–12
Chang et al. [5]	smooth-rec micro-rec	3.21, 3.18 N/A	7,6 5	R-22, R-134a	30–100	40,45	N/A
Wang et al. [6]	smooth-rec	1.46	10	R-134a	150–750	62–66	N/A
Zhang and Webb [7]	smooth-cir	2.13	8	R-134a, R-22 R-404a	400–1000	25–65	N/A
Kim et al. [8]	smooth-rec	1.41	7	R-22, R-410A	200–600	45	10
Webb and Ermis [9]	smooth-rec micro-rec	1.33 0.61, 1.56 0.44	10 11,4 18	R-134a	300–1000	65	8
Koyama et al. [10]	smooth-rec	1.36, 0.8	8, 19	R-134a	100–700	65	N/A
Cavallini et al. [11]	smooth-rec	1.4	13	R-134a, R-410A	200–1400	40	N/A
Bandhauer et al. [12]	smooth-cir	1.52, 0.76 0.51	10, 17, 23	R-134a	150–750	55	N/A
Agrawal et al. [13]	smooth-rec smooth-barrel smooth-triang	0.76, 0.42 0.80 0.84 0.73 0.54	17, 20 14 19 19 19	R-134a	150–750	55	N/A
Park et al. [14]	smooth-W smooth-N	1.45	7	R-1234ze(E)	100–250	30–70	26–36
Sakamatapan et al. [15]	smooth-rec	1.1, 1.2	14, 8	R-134a, R-236fa	340–680	35–45	15–25
Illan-Gomez et al. [16]	smooth-rec	1.16	10	R-134a	275–940	25–55	N/A
Lopez-Belchi et al. [17]	smooth-rec	1.16	10	R-1234yf R-134a	475–800	30–50	N/A
Park and Hrnjak [18]	smooth-rec	0.89	10	R-32, R-410A	200–800	–15–25	N/A
Heo et al. [19]	smooth-cir	1.5, 0.78, 0.68	7, 23, 19	CO <sub>2</sub> CO <sub>2</sub>	400–800	–5–5	N/A
Fernando et al. [20]	smooth-rec	1.42	6	propane	19–53	30–50	N/A

a smooth multi-port tube of  $D_h = 1.46$  mm having 10 channels using R-134a. The test range covered  $150 \leq G \leq 750$  kg/m<sup>2</sup> s,  $61.5 \leq T_{\text{sat}} \leq 66$  °C. When the heat transfer data are compared with predictions of existing correlations, Akers et al. [21] correlation turned out to be the best. A new correlation, which covers both the annular and stratified flow regime, was proposed. Zhang and Webb [7] developed a friction correlation based on reduced pressure concept.

Kim et al. [8] provided condensation heat transfer data for the smooth ( $D_h = 1.41$  mm, 7 channels) and micro-finned ( $D_h = 1.56$  mm, 4 channels) multi-port tubes using R-22 and R-410A. The test range covered  $200 \leq G \leq 600$  kg/m<sup>2</sup> s at  $q = 10$  kW/m<sup>2</sup> and  $T_{\text{sat}} = 45$  °C. They noted that Akers et al. [21] correlation reasonably predicted the condensation heat transfer data. Heat transfer enhancement by microfins was dependent on the refrigerant. For R-22, the microfin tube yielded higher heat transfer coefficients. For R-410A, however, the reverse was true. The applicability of Akers et al. [21] correlation for multi-port tubes has further been confirmed by Webb and Ermis [9], where tubes having a wide range of hydraulic diameters (from 0.44 mm to 1.56 mm, smooth and microfin) were tested. Their test range covered  $300 \leq G \leq 1000$  kg/m<sup>2</sup> s at  $q = 8$  kW/m<sup>2</sup> and  $T_{\text{sat}} = 60$  °C. Koyama et al. [10] investigated R-134a condensation in smooth multi-port tubes with  $D_h = 1.36$  mm (8 channels) and 0.8 mm (19 channels) for the test range  $100 \leq G \leq 400$  kg/m<sup>2</sup> s at  $T_{\text{sat}} = 65$  °C. Comparison of the data with Moser et al. [24] correlation based on equivalent Reynolds number was not satisfactory, and they developed a new correlation extending Haraguchi et al. [25] correlation. The friction data were well predicted by Mishima and Hibiki [26] correlation.

Cavallini et al. [11] obtained condensation heat transfer and pressure drop data of R-134a and R-410A for a smooth multi-port tube ( $D_h = 1.4$  mm, 13 channels) for the test range  $200 \leq G \leq 1400$  kg/m<sup>2</sup> s at  $T_{\text{sat}} = 40$  °C. R-410A yielded higher pressure drop and heat transfer coefficient compared with R-134a. They suggested a heat transfer model for condensation inside multi-port tubes, based on an analogy between heat and momentum transfer. Bandhauer et al. [12] tested three smooth multi-port tubes ( $0.51 \leq D_h \leq 1.52$  mm) having circular cross-section using R-134a. The test range covered  $150 \leq G \leq 750$  kg/m<sup>2</sup> s at  $T_{\text{sat}} = 55$  °C. The condensation heat transfer coefficient increased as the tube hydraulic diameter decreased. Comparison of the data with available correlations revealed that Moser et al. [24] correlation performed best. A new heat transfer model based on boundary layer analysis was proposed. Their study was extended to non-circular multi-port tubes having various cross-sectional shapes (square, barrel, triangular, rectangular, W-shaped, N-shaped) by Agarwal et al. [13]. Park et al. [14] obtained condensation heat transfer coefficients of R-1234ze(E), R-134a and R-236fa in a smooth multi-port tube having  $D_h = 1.45$  mm for the test range  $100 \leq G \leq 250$  kg/m<sup>2</sup> s,  $26 \leq q \leq 36$  kW/m<sup>2</sup> and  $30 \leq T_{\text{sat}} \leq 70$  °C.

The heat transfer coefficients of R-1234ze(E) were 15 to 25% lower than those of R-134a, but relatively similar to those of R-236fa. Comparison of the data with existing correlations was not satisfactory, and a new correlation was proposed. Sakamatapan et al. [15] tested two smooth multi-port tubes ( $D_h = 1.1$  and 1.2 mm) using R-134a for the test range  $340 \leq G \leq 680$  kg/m<sup>2</sup> s,  $15 \leq q \leq 25$  kW/m<sup>2</sup> at  $35 \leq T_{\text{sat}} \leq 45$  °C. Comparison of the data with Webb et al. [27] correlation was satisfactory. Illan-Gomez et al. [16] compared condensation heat transfer coefficients and pressure drops of R-1234yf and R-134a in a smooth multi-port tube having  $D_h = 1.16$  mm. The test range covered  $275 \leq G \leq 940$  kg/m<sup>2</sup> s,  $25 \leq T_{\text{sat}} \leq 55$  °C. R-134a yielded higher heat transfer coefficient and higher pressure drops. Lopez-Belchi et al. [17] extended the study to R-32 and R-410A. R-32 yielded higher heat transfer coefficient and higher pressure drops. Additional studies on condensation heat transfer of CO<sub>2</sub> in multi-port tubes were reported by Park and Hrnjak [18] and Heo et al. [19]. Fernando et al. [20] investigated the condensation heat transfer performance of propane in a multi-port tube. A review on the prediction methods for the pressure drop in a multi-port tube was provided by Yun and Jeong [28].

As mentioned, brazed aluminum heat exchangers which use multi-port tubes have long been used as condensers of automotive air-conditioning units, where R-134a is a refrigerating fluid. Thus, most of the condensation studies have been conducted using R-134a. Recently, brazed aluminum heat exchangers are commonly used as condensers of residential air-conditioning systems, where R-410A is a refrigerating fluid. Table 1 shows that only three studies [8, 11, 17] are available for condensation of R-410A in a multi-port tube. These studies are, however, limited to  $D_h$  larger than 1 mm, relatively large mass flux ( $200 \leq G \leq 1400$  kg/m<sup>2</sup> s) and relatively large heat flux ( $q \cong 10$  kW/m<sup>2</sup>). Typical mass flux and heat flux of the residential condenser are  $100 \leq G \leq 400$  kg/m<sup>2</sup> s and  $q \cong 3$  kW/m<sup>2</sup> [29]. In addition, recent trend of the multi-port tube is to use reduced hydraulic diameter tubes. In this study, R-410A condensation tests were conducted in four smooth multi-port tubes having a range of hydraulic diameter ( $0.78 \leq D_h \leq 0.95$  mm). The effect of hydraulic diameter on condensation heat transfer of R-410A is discussed. The test range covered the mass flux from 100 to 400 kg/m<sup>2</sup> s and the heat flux was fixed at 3 kW/m<sup>2</sup>. The saturation temperature was maintained at 45° C.

## 2 Experimental apparatus

Schematic drawings of the multi-port tubes tested in this study are shown in Fig. 1, and geometric details are listed in Table 2. Tubes are designated by a set of hydraulic diameter - number of channels. For example, 0.78–18 tube has 0.78 mm hydraulic diameter and 18 channels. Four tubes have different

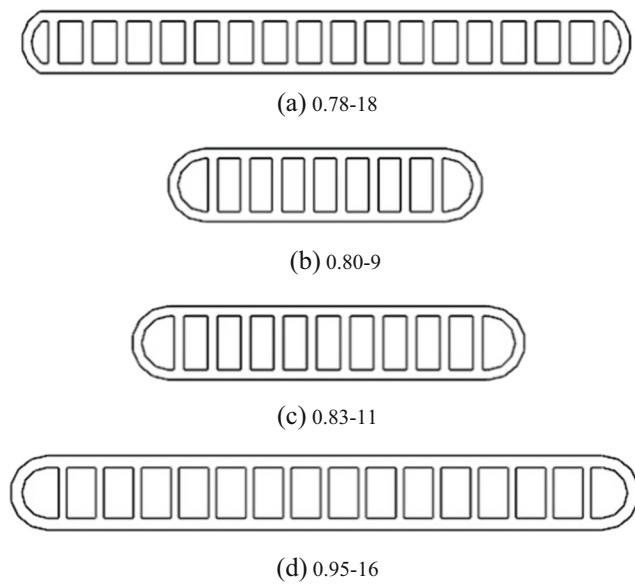


**Fig. 1** Flat multi-port tubes tested in this study

hydraulic diameter, number of channels and aspect ratios. As mentioned, the hydraulic diameter ranged from 0.78 to 0.95 mm. Numbers of channels of the four tubes are widely different - from 9 to 18. Aspect ratios of 0.95–16 and 0.78–18 tube are approximately the same, and those of 0.80–9 and 0.83–11 tube are approximately similar. This complexity of tube dimensions was unavoidable due to the availability of the tubes from the market.

A schematic drawing of the apparatus is shown in Fig. 2, and a detailed drawing of the test section and photos of the tube are shown in Fig. 3. The same apparatus and test section by Kim et al. [8] were used in the present study. The apparatus has been successfully used to obtain the smooth tube condensation data [30]. The test section comprises of a flat tube and an annular channel with a length of 455 mm. Fig. 3a shows the cross-sectional view of the test section. The refrigerant flows inside of the tube and the cooling water flows in the annular channel. Fig. 3b shows a photo of the tube with brazed transition sections. Fig. 3c shows the end view of the tube sample, where thin wire of 0.3 mm was wrapped with 3.0 mm pitch

**Table 2** Geometric details of the multi-port flat tubes

Item	0.78–18	0.80–9	0.83–11	0.95–16
$w$ (mm)	16.0	8.0	10.0	16.0
$b$ (mm)	1.5	1.8	1.8	1.8
$A_c$ (mm <sup>2</sup> )	10.5	6.21	8.13	13.2
$P_w$ (mm)	53.9	31.1	39.0	55.6
$D_h$ (mm)	0.78	0.80	0.83	0.95
$t$ (mm)	0.25	0.25	0.25	0.3
$AR$	1.72	2.41	2.32	1.71
$N$	18	9	11	16

around the tube. Each tube had separate transition sections due to different tube width. Smooth transition from the flat tube and the round tube of 6.0 mm diameter was accomplished by the transition tube [Fig. 3d] of 20 mm diameter and 150 mm length. For an accurate measurement of tube-side condensation heat transfer coefficient, it is important to minimize the thermal resistance of the annular side. This was accomplished by increasing the annular-side water velocity, and by wrapping thin wire around the tube. To increase the water velocity, the annular gap was maintained small (1.0 mm).

As illustrated in Fig. 2, the refrigerant flows into the test section at a known quality and partly condenses in the test section by an annular-side cooling water. Two-phase refrigerant mixture from the test section enters the separator, where the liquid drains down to the receiver and the vapor flows into the upper shell-and-tube condenser. The condensed liquid drains down to the receiver. The sub-cooled liquid passes through the magnetic gear pump, mass flow meter, and enters the pre-heater. The refrigerant flow rate was controlled by by-passing an appropriate amount of liquid. The vapor quality into the test section was controlled by the heat input supplied to the pre-heater. The heat flux to the flat tube was controlled by changing the temperature of the cooling water. The flow rate of the cooling water was fixed at 1.0 l per minute throughout the test.

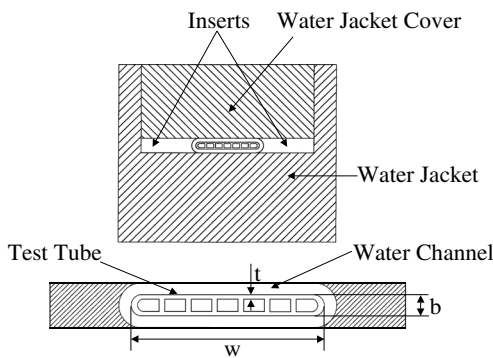
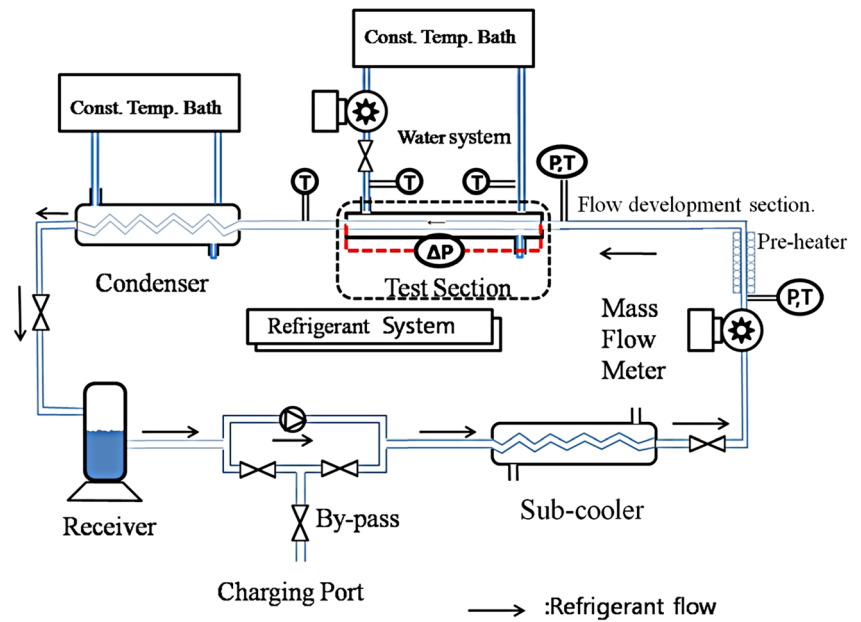
Temperatures were measured at five locations; refrigerant temperatures at inlet and outlet of the test tube, cooling water temperatures at inlet and outlet of the annular channel and a sub-cooled refrigerant temperature at the inlet of the pre-heater. Thermowells having five thermocouples each were used to measure local temperatures. Two absolute pressures were measured - one at the inlet of the test section, and the other at the inlet of the pre-heater. These absolute pressures were used to check the state (sub-cooled or saturated) of the refrigerant. A differential pressure transducer was used to measure the pressure drop across the test section. The refrigerant and water flow rates were measured by mass flow meters (Micromotion: DN25S-SS-1) with  $\pm 1.5 \times 10^{-6}$  m<sup>3</sup>/s accuracy.

The saturation pressure corresponding to the saturation temperature 45 °C is 27 bar and the apparatus was checked for leak-tight. Leak tests were conducted by a soap bubble technique followed by a halogen leak detection. The leakage resulted in a decrease in pressure less than 0.5 kPa per hour. The condensation test started at the maximum mass flux. After the system was stabilized, quality (from 0.2 to 0.8) and mass flux (from 100 to 400 kg/m<sup>2</sup> s) were sequentially varied, all in a decreasing manner. The heat flux was fixed at 3 kW/m<sup>2</sup> and the saturation temperature was maintained at 45 °C.

### 3 Data reduction

From the measured data, the overall heat transfer coefficient  $U_o$  is obtained from the following equations. Here,  $m_w$  is the

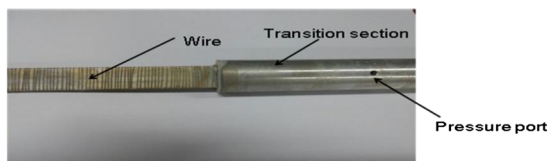
**Fig. 2** Schematic drawing of the experimental apparatus



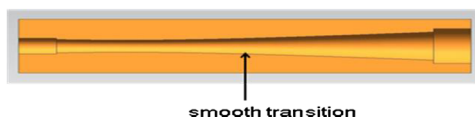
(a) Cross-sectional view of the test section



(b) Photo of the test tube



(c) End view of the test tube



(d) Sketch of the transition section

**Fig. 3** Detailed drawing of the test section

water flow rate,  $c_{pw}$  is the specific heat of water,  $T_{w,out}$  and  $T_{w,in}$  is the water outlet and inlet temperature,  $T_{r,out}$  and  $T_{r,in}$  is the refrigerant outlet and inlet temperature

$$Q = m_w c_{pw} (T_{w,out} - T_{w,in}) = U_o A_o \Delta T_{lm} \quad (1)$$

$$\Delta T_{lm} = \frac{(T_{w,in} - T_{r,in}) - (T_{w,out} - T_{r,out})}{\ln \frac{(T_{w,in} - T_{r,in})}{(T_{w,out} - T_{r,out})}} \quad (2)$$

The tube-side condensation coefficient  $h_i$  is determined from Eq. (3) using the overall heat transfer coefficient  $U_o$  and the annular-side heat transfer coefficient  $h_o$ . Here,  $A_i$  is the internal surface area,  $A_o$  is the outer surface area,  $A_m$  is the area at the middle plane of tube wall (excluding internal web).

$$h_i = \left[ \left( \frac{1}{U_o} - \frac{1}{h_o} \right) \frac{A_i}{A_o} - \frac{t A_i}{k A_m} \right]^{-1} \quad (3)$$

The annular-side heat transfer coefficient  $h_o$  was determined from the Wilson plot [31]. Wilson plot method is graphically illustrated in Fig. 4. In the Wilson plot method, tests are conducted increasing tube-side velocity ( $V$ ), and  $1/UA$  values are drawn as a function of  $V^{0.8}$ . At an infinite velocity, which is obtained by extrapolating the  $1/UA$  line, tube-side thermal resistance  $1/h_i A_i$  becomes zero and  $1/UA$  equals  $1/h_o A_o + t/k A_m$ , where  $h_o$  is readily calculated. One thing to be careful when running a Wilson plot test is that the annulus-side water temperature should be kept constant, which is realized by controlling the water temperature out of the constant water temperature bath.

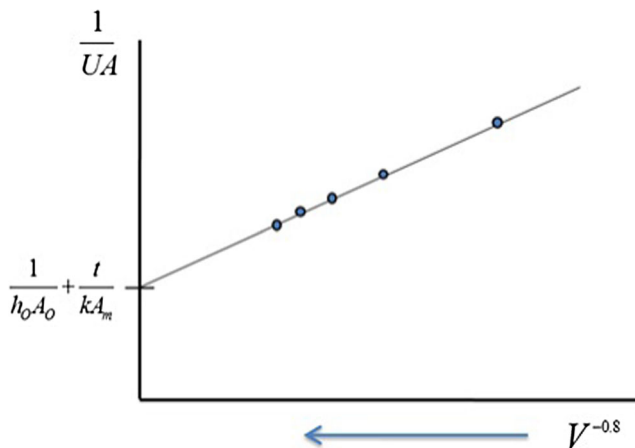


Fig. 4 Graphical interpretation of the Wilson plot [31]

Other important thing to run a Wilson plot test is to maintain both tube-side and annulus-side turbulent. To promote turbulence at the annulus-side, thin wire of 0.3 mm diameter was wrapped around the tube at 2.0 mm pitch. Heat balances between the tube-side and annulus-side were checked during Wilson plot tests, which were less than  $\pm 3.0\%$  for the entire test range. Tests were conducted changing annulus-side water velocity and temperature to obtain exponents of Reynolds number and Prandtl number. The resulting annulus-side forced convection equation is as follows.

$$Nu_{Dh} = 0.141 Re_{Dh}^{0.70} Pr_w^{0.4} (0.78-18) \quad (4)$$

$$Nu_{Dh} = 0.173 Re_{Dh}^{0.68} Pr_w^{0.4} (0.89-9) \quad (5)$$

$$Nu_{Dh} = 0.058 Re_{Dh}^{0.82} Pr_w^{0.4} (0.83-11) \quad (6)$$

$$Nu_{Dh} = 0.041 Re_{Dh}^{0.86} Pr_w^{0.4} (0.96-16) \quad (7)$$

Eqs. (4) to (7) are applicable for  $2400 \leq Re_{Dh} \leq 5200$ . To obtain reliable heat transfer data from tests using Wilson plot, it is important to minimize the Wilson-plot-side thermal resistance. For the present test, approximately 1/3 of total thermal resistance was on the annular-side. This portion may be reduced by increasing the flow velocity. In that case, however, the temperature difference between inlet and outlet becomes small, and the uncertainty on the heat supplied to the test section increases. An approximate optimum annular-side water flow rate, which balanced the water temperature difference and the thermal resistance, was found (1.0 l per minute) by trial and error with corresponding Reynolds number of approximately 4600. At this water flow rate, the water temperature difference from inlet to outlet was larger than  $0.7^\circ\text{C}$ , which was obtained at the lowest mass flux ( $G = 100 \text{ kg/}$

$\text{m}^2 \text{ s}$ ), and the annular-side thermal resistance was less than 1/3 of the total resistance for the entire test range. The average vapor quality in the test tube is determined from Eq. (8).

$$x_{ave} = x_{in} - \Delta x / 2 \quad (8)$$

$$\Delta x = \frac{m_w c_{pw} (T_{w,out} - T_{w,in})}{m_r i_{fg}} \quad (9)$$

Here,  $\Delta x$  is the change of vapor quality across the test section,  $m_r$  is the refrigerant flow rate,  $i_{fg}$  is the latent heat of the refrigerant. The amount of  $\Delta x$  ranged from 0.13 to 0.52. It increased as mass flux decreased. In Eq. (10),  $Q_p$  is the heat supplied to the pre-heater,  $T_{p,in}$  is the liquid refrigerant temperature into the pre-heater and  $c_{pr}$  is the specific heat of the liquid refrigerant. Sub-cooled liquid out of the pump was supplied to the pre-heater.

$$x_{in} = \frac{1}{i_{fg}} \left[ \frac{Q_p}{m_r} - c_{pr} (T_{sat} - T_{p,in}) \right] \quad (10)$$

For two-phase flow, the total pressure gradient comprises of three terms - frictional, accelerational and gravitational pressure gradient.

$$\frac{dP}{dz} = \left( \frac{dP}{dz} \right)_f + \left( \frac{dP}{dz} \right)_a + \left( \frac{dP}{dz} \right)_g \quad (11)$$

Then, the frictional pressure gradient may be obtained by subtracting the accelerational pressure gradient from the measured total pressure gradient. In the present setup, gravitational pressure gradient is zero because the test section is under horizontal position. The accelerational pressure gradient obtained from Collier and Thome [32] is

$$\left( \frac{dP}{dz} \right)_a = G^2 \frac{d}{dz} \left[ \frac{x^2 v_g}{\alpha} + \frac{(1-x)^2 v_f}{(1-\alpha)} \right] \quad (12)$$

where the void fraction  $\alpha$  is obtained from Zivi [33]. According to Kline and McClintock [34], when a parameter 'R' is a function of measured variables ( $x_1, x_2, \dots, x_n$ ), the uncertainty on the parameter 'w<sub>R</sub>' is obtained from the following equation.

$$w_R = \left[ \left( \frac{\partial R}{\partial x_1} w_1 \right)^2 + \left( \frac{\partial R}{\partial x_2} w_2 \right)^2 + \dots + \left( \frac{\partial R}{\partial x_n} w_n \right)^2 \right]^{1/2} \quad (13)$$

Here, 'w<sub>1</sub>' is the uncertainty on variable 'x<sub>1</sub>', 'w<sub>2</sub>' is the uncertainty on variable 'x<sub>2</sub>', etc. As an example, the

**Table 3** Experimental uncertainties

Parameter	Uncertainties
Temperature	$\pm 0.1$ °C
Pressure	$\pm 0.02$ kPa
Water flow rate	$\pm 0.2\%$
Refrigerant flow rate	$\pm 0.1\%$
Heat flux	$\pm 2.7\%$
Vapor quality	$\pm 1.0\%$
$h_o$	$\pm 10.0\%$
$h_i$	$\pm 11.1\% \sim \pm 13.0\%$
$(dP/dz)_f$	$\pm 0.2\% \sim \pm 4.3\%$

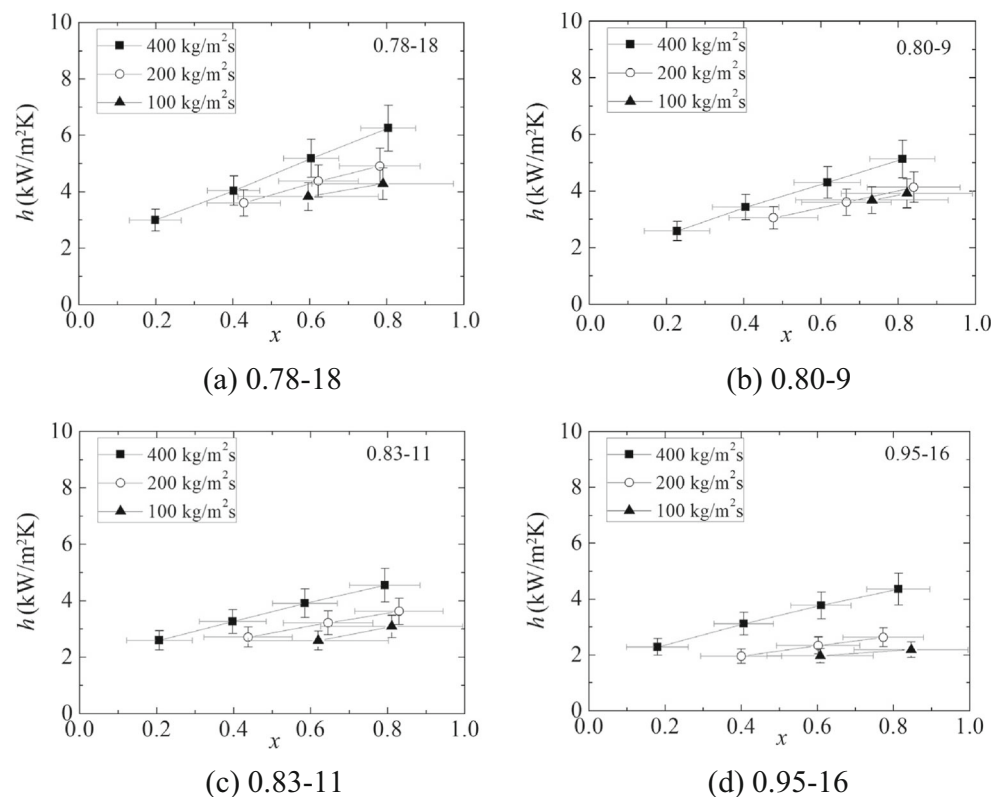
uncertainty on evaporation heat transfer coefficient is obtained as follows. From Eqs. (1), (3) and (13),

$$\frac{w_{hi}}{h_i} = \left[ \left( \frac{h_o}{h_o - U_o} \frac{w_{U_o}}{U_o} \right)^2 + \left( \frac{-U_o}{h_o - U_o} \frac{w_{h_o}}{h_o} \right)^2 \right]^{1/2} \quad (14)$$

$$\frac{w_{U_o}}{U_o} = \left[ \left( \frac{w_q}{q} \right)^2 + \left( \frac{w_{\Delta T_{lm}}}{\Delta T_{lm}} \right)^2 \right]^{1/2} \quad (15)$$

$$\frac{w_{\Delta T_{lm}}}{\Delta T_{lm}} = \frac{1}{\Delta T_{lm}} \left[ \left( \frac{w_{T_{r,in}}}{2} \right)^2 + \left( \frac{w_{T_{r,out}}}{2} \right)^2 + \left( \frac{w_{T_{w,in}}}{2} \right)^2 + \left( \frac{w_{T_{w,out}}}{2} \right)^2 \right]^{1/2} \quad (16)$$

**Fig. 5** Condensation heat transfer coefficients of the tested tubes showing the effect of mass flux



Introducing the measurement uncertainties listed in Table 3 and assuming an uncertainty on Wilson plot  $w_{h_o}/h_o$  to be  $\pm 10.0\%$ , the uncertainties on the heat transfer coefficients are  $\pm 11.1 \sim \pm 13.0\%$ , and those of pressure drops are  $\pm 0.2 \sim \pm 4.3\%$ . All the uncertainties are based on 95% confidence level. The uncertainty increased as the mass flux or vapor quality decreased.

## 4 Results and discussions

In Fig. 5, condensation heat transfer coefficients of the four tubes are shown as a function of mass flux. At the lowest mass flux of 100 kg/m<sup>2</sup> s, low quality data missing due to difficulty of obtaining the data. At the low quality, the exit quality of the test section was negative (liquid). Error bars for the heat transfer coefficients and qualities are also drawn in the figure. Fig. 5 shows that the heat transfer coefficient increases as mass flux or quality increases. This is a general trend of condensation heat transfer. As mass flux or quality increases, the flow momentum increases, which results in higher heat transfer coefficient.

For two-phase flow, the heat transfer coefficient and the pressure drop are significantly affected by the flow pattern. Thus, it is necessary to identify the flow regime for the entire test range. In Fig. 6, tested mass fluxes and qualities are marked in the flow pattern map of Garimella [35]. Garimella map was made based on the flow visualization of R-134a in a

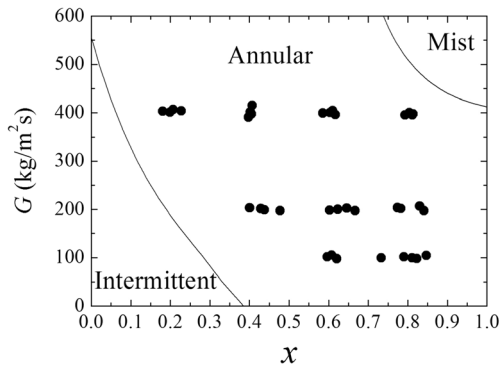


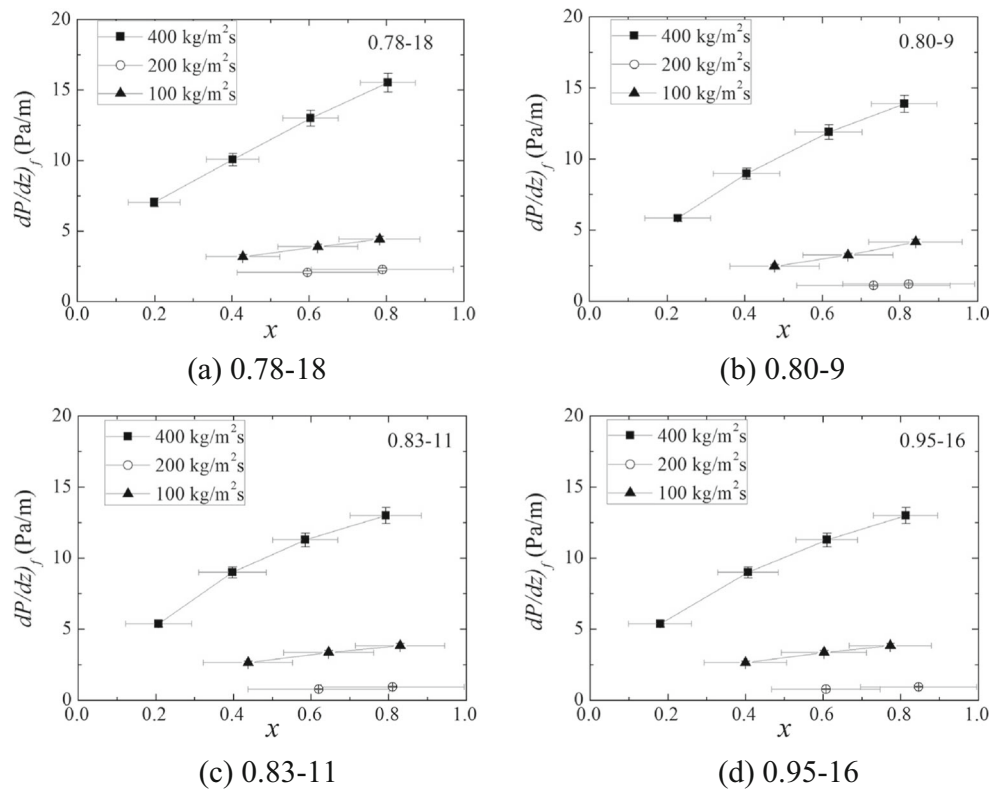
**Fig. 6** Flow pattern of the present study shown in the map of Garimella [35]

1.0 mm circular channel. Garimella noted that the flow pattern in a rectangular channel, which is of interest in the present study, was approximately the same as that in a circular channel. Although the present study was conducted using R-410A, the flow pattern would be approximately the same as that obtained using R-134a, considering that the liquid and gas density ratio of R-410A is not significantly different from that of R-134a (8.0 for R-410A and 20.2 for R-134a at 45 °C saturation temperature). The liquid and gas density ratio may be the most influential parameter, which determines the flow pattern. Also worth noting is that Garimella map was based on a single tube. At present, no flow pattern map is available for a multi-port tube. Fig. 6 shows that the flow pattern of the

present study belongs to annular even at the lowest mass flux of  $100 \text{ kg/m}^2 \text{ s}$ . In Fig. 7, the frictional pressure gradients of the four tubes are shown along with error bars. As expected, the pressure gradient increased as mass flux or quality increased.

In Fig. 8, the heat transfer coefficients are re-grouped to show the effect of tube geometry on heat transfer coefficient. For all mass fluxes, the heat transfer coefficient increased as tube hydraulic diameter decreased. The difference was more evident at a lower mass flux. Also shown in the figure are heat transfer coefficients obtained by Kim et al. [8] for the multi-port tube of 1.41 mm hydraulic diameter using the same refrigerant R-410A. One thing to be noted is that Kim et al.'s [8] data were obtained at  $10 \text{ kW/m}^2$  heat flux, which is much higher than the present heat flux of  $3 \text{ kW/m}^2$ . The original Kim et al. data (shown as a dark solid line) lie between those of  $D_h = 0.80 \text{ mm}$  (0.80–9) and  $0.83 \text{ mm}$  (0.83–11). The effect of heat flux on condensation heat transfer coefficient in multi-port tubes were investigated by Yang and Webb [2], who reported that the heat transfer coefficient increased as the heat flux increased with the heat flux dependency of  $q^{0.2}$ . Kim et al.'s [8] data were adjusted to the lower heat flux of  $3 \text{ kW/m}^2$  using the heat flux dependency of  $q^{0.2}$ , and the results are shown in Fig. 8 as a dotted line. The adjusted data are indeed lower than those of the present tubes, supporting the argument that the heat transfer coefficient decreased as the hydraulic diameter increased. In Fig. 9, the frictional pressure gradients

**Fig. 7** Frictional pressure gradients of the tested tubes showing the effect of mass flux





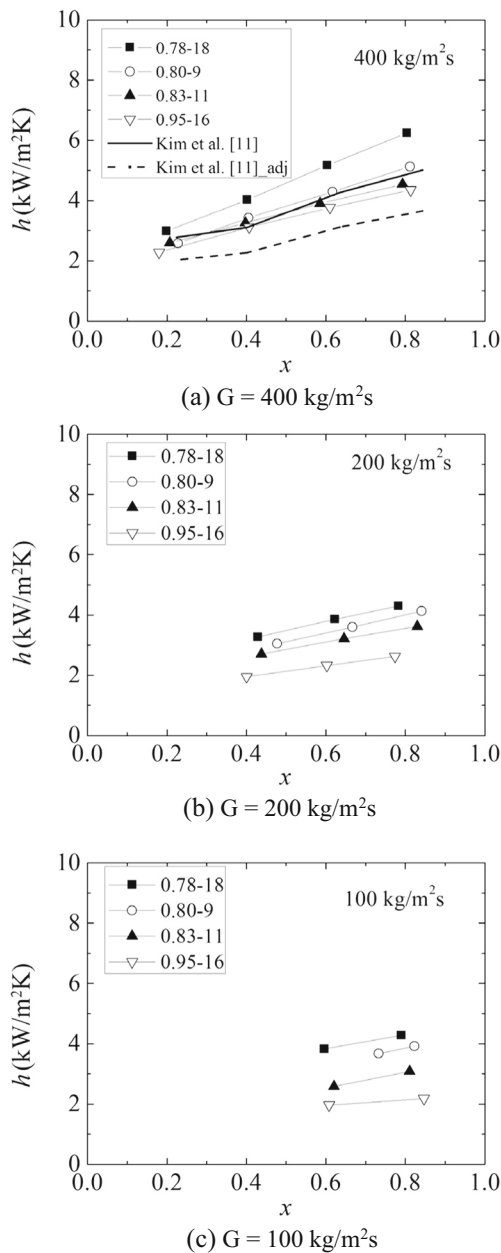


**Fig. 8** Condensation heat transfer coefficients of the tested tubes showing the effect of tube geometry

are re-drawn to elucidate the effect of tube diameter. Generally, pressure gradient increased as hydraulic diameter decreased. The effect is most pronounced for the tube having the smallest hydraulic diameter (0.78–18).

For condensation in a multi-port tube, flow mal-distribution between the ports may occur. The flow mal-distribution increases the pressure drop and reduces the heat transfer. The effect of flow mal-distribution on condensation heat transfer has been theoretically studied by Lopez-Belchi et al. [36], who showed that the heat transfer could be significantly reduced (up to 70%) by the mal-distribution. They obtained possible two-phase flow profiles which satisfied the

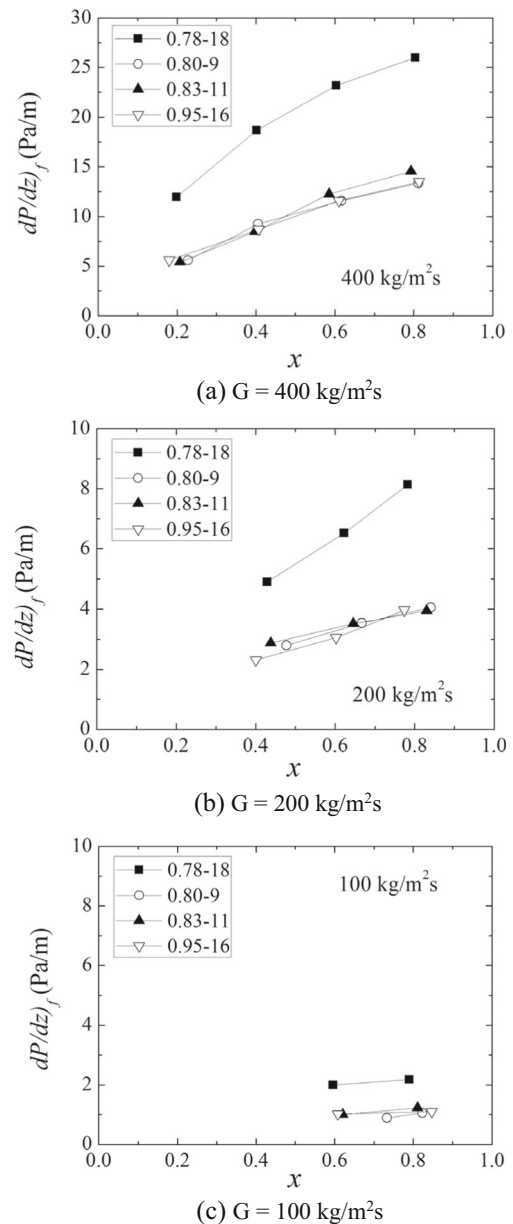


**Fig. 9** Frictional pressure gradients of the tested tubes showing the effect of tube geometry

equal pressure drop constraint, and compared the heat transfer rates. Pressure drop increase by the mal-distribution, however, was not assessed. The effect of flow mal-distribution on pressure drop may be assessed if a mal-distribution profile is given. As an extreme case, consider a single phase liquid and assume that all the liquid flows into a single port. Then, the velocity in that port will be  $N$  times ( $N$ : number of port) of the average value. The pressure drop increase will approximately be  $N^2$  whereas the heat transfer increase is approximately  $N^{0.8}$ . Then, we may roughly conclude that the effect of flow mal-distribution is more severe on pressure drop than on the heat transfer. This may explain the different hydraulic diameter behavior between heat transfer and pressure drop (Figs. 8

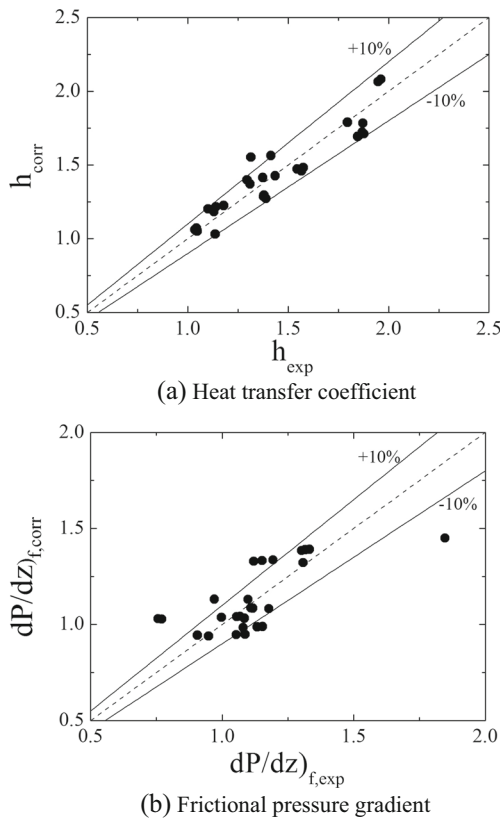


**Fig. 10** Present data compared with Eqs. (10) and (11)

and 9). As shown in Fig. 1,  $D_h = 0.78$  mm (0.78–18) and 0.95 mm (0.95–16) tubes have larger number of ports than other tubes (0.80–9 and 0.83–11). Considering that maldistribution will be larger for the tubes having larger number of ports, the pressure drop increase of the 0.78–18 and 0.95–16 tubes over other tubes will be more apparent than that of the heat transfer counterpart. This may explain the exceptionally large pressure drop for the 0.78–18 tube and approximately equal (with 0.80–9 and 0.83–11) pressure drop of the 0.96–16 tube (Fig. 9), and the gradual increase of the heat transfer coefficients with decrease of the hydraulic diameter (Fig. 8).

To deduce the effect of hydraulic diameter on heat transfer coefficient, the data were normalized by those of the largest hydraulic diameter ( $D_h = 0.95$  mm). The correlating variables are  $D_h$ ,  $N$ ,  $G$  and  $x$ . Listed below is the derived correlation.

$$\frac{h}{h_{0.95}} = 2.19D_h^{-4.03}G^{-0.27}x^{0.03}N^{0.07} \tag{17}$$

Fig. 10a shows that the correlation predicted the experimental results within  $\pm 10\%$ . Eq. (17) reveals that hydraulic diameter dependency of the heat transfer coefficient is very strong. The effect of hydraulic diameter on condensation heat transfer in a multi-port tube has been investigated by Webb and Ermis [9] for the test range  $300 \leq G \leq 1000$  kg/m<sup>2</sup> s at  $q = 8$  kW/m<sup>2</sup> and  $T_{sat} = 60$  °C using R-134a. Their multi-port

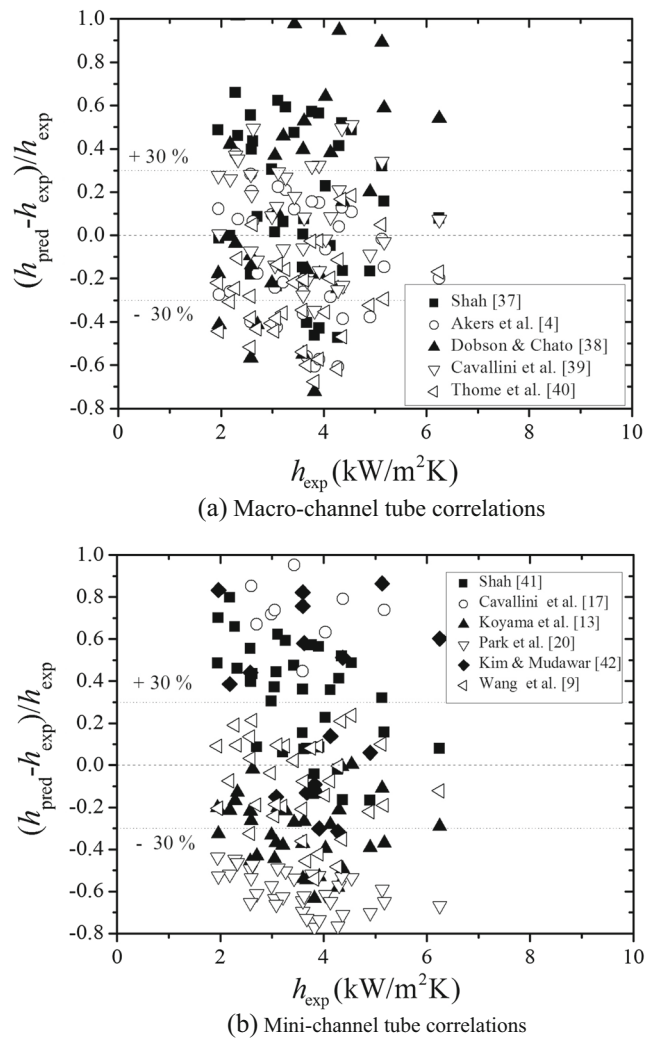


**Fig. 11** Present heat transfer coefficients compared macro- and mini-channel tube correlations

tubes had a range of hydraulic diameter (from 0.44 to 1.56 mm) with 4 to 12 sub-channels. From the test results, they recommended Akers et al. [21] correlation to predict the condensation heat transfer in a multiport tube. The Akers et al. [21] correlation suggests heat transfer coefficient to be proportional to  $D_h^{-0.2}$ . This hydraulic diameter dependency is much weaker than the present results (Eq. 10). The range of the hydraulic diameter of the present study is rather narrow (from 0.78 to 0.95 mm), and the present results should be considered with caution. Addition of Kim et al. [8] data of  $D_h = 1.41$  mm mitigates the hydraulic diameter dependency to  $D_h^{-0.5}$ .

Similar attempt was made on the pressure drop. The derived correlation is as follows.

$$\frac{dP/dz_f}{dP/dz_{f,0.95}} = 0.40D_h^{-3.75}G^{-0.06}x^{0.01}N^{0.22} \tag{18}$$

**Table 4** RMS errors of the correlations

	h	RMSE	dp/dz <sub>f</sub>	RMSE
Macro-channel	Shah [37]	37.5	Cavallini et al. [39]	112
	Akers et al. [21]	29.6	Jung and Radermacher [43]	389
	Dobson and Chato [38]	68.1	Friedel [44]	223
	Cavallini et al. [39]	25.3	Muller-Steinhagen and Heck [45]	104
	Thome et al. [40]	35.3		
Mini-channel	Shah [41]	41.1	Cavallini et al. [46]	28.5
	Cavallini et al. [11]	167	Kim and Mudawar [42]	66.3
	Koyama et al. [10]	34.5	Sun and Mishima [47]	108
	Park et al. [14]	60.3	Lopez-Belchi et al. [17]	112
	Kim and Mudawar [42]	181	Zhang and Webb [7]	68.5
	Wang et al. [6]	23.1		

Fig. 10b shows that the correlation predicted most of the experimental results within  $\pm 10\%$ . Eq. (18) reveals that hydraulic diameter dependency of the pressure drop is also very strong. In addition, the exponent of  $N$  (number of ports) is not small. This value was quite small for heat transfer counterpart [Eq. (14)]. Considering that the exponent of  $N$  implies the amount of flow mal-distribution in the multi-port tube, larger exponent of  $N$  for the pressure drop correlation further supports the argument proposed in the previous section that the effect of flow mal-distribution is more severe on pressure drop than on heat transfer.

The literature survey reveals many condensation heat transfer and pressure drop correlations. The correlations may be grouped to those for macro-channel tubes and those for mini-channel tubes. Heat transfer correlations for macro-channel tubes include Akers et al. [21], Shah [37], Dobson and Chato [38], Cavallini et al. [39] and Thome et al. [40]. Heat transfer correlations for mini-channel tubes include Wang et al. [6], Koyama et al. [10], Cavallini et al. [11], Park et al. [14], Shah [41], Kim and Mudawar [42]. All these correlations are applicable to annular flow regime, which is the flow regime of this study. This paper addresses three Shah [22, 37, 41] correlations. Shah [37] updated his original version [22] to cover new refrigerants including R-410A. Recently, a separate correlation for condensation heat transfer in a mini-channel was proposed [41]. Experimental heat transfer coefficients are compared with the predictions of the correlations in Fig. 11, and RMS errors are summarized in Table 4. Fig. 11a shows that some correlations for macro-channel tubes, Cavallini et al. [39], Akers et al. [21], Thome et al. [40] and Shah [37] reasonably predict the data. Especially, Cavallini et al. [39] correlation predicts the data with 25.5% RMS error. Of the mini-channel correlations, Wang et al. [6] and Koyama et al. [10] correlations reasonably predict the data, with 23.1% RMS error by Wang et al. [6] correlation.

Predictions of all the correlations showed minimal effect of hydraulic diameter on heat transfer coefficient. The heat transfer coefficients were approximately proportional to  $D_h^{-0.2}$ . When the exponent ( $-0.2$ ) was applied to the present range of hydraulic

diameter (0.78 to 0.95 mm), the difference of heat transfer coefficient between the largest (0.78 mm) and the smallest (0.95 mm) one was only 4%. This result is significantly different from the experimental data shown in Fig. 8 and Eq. (14). More supporting data are needed to clear this issue. One thing to be mentioned is that the present multi-port tubes had different number of channels and different channels aspect ratio as shown in Table 1. Number of channels or channel aspect ratio may affect the heat transfer performance by many ways. Flow non-uniformity between channels may occur in multi-port tubes, and the amount may be affected by number of channels. This may be true if the number of channels is significantly different. For the present study, every effort was made to provide uniform flow to each channel, for example, by providing a long (150 mm) smooth transition section at inlet of the sample tube. However, flow mal-distribution may have occurred, which degrades the heat transfer performance. Next, channel aspect ratio will affect the condensation heat transfer performance of a multi-port tube. The aspect ratio of the present samples ranged from 1.71 to 2.41. Thus, number of channels and channel aspect ratio may also be responsible for the difference in the heat transfer coefficient of the present study in addition to the hydraulic diameter.

Pressure drop correlations may also be divided into two categories - those for macro-channel tubes and those for mini-channel tubes. Macro-channel correlations include Cavallini et al. [39], Friedel [44], Jung and Radermacher [43], Muller-Steinhagen and Heck [45]. Mini-channel correlations include Cavallini et al. [46], Kim and Mudawar [42], Sun and Mishima [47], Lopez-Belchi et al. [17], Zhang and Webb [7]. All these correlations are applicable to annular flow regime. The present frictional pressure drop data are compared with the correlations, and the results are shown in Fig. 12, and RMS errors are summarized in Table 4. Fig. 12a shows that, in general, macro-channel tube correlations overpredict the data. Fig. 12b shows that some mini-channel tube correlations reasonably predict the data. Especially, Cavallini et al. [46] correlation predicts the data with 28.5% RMS error.

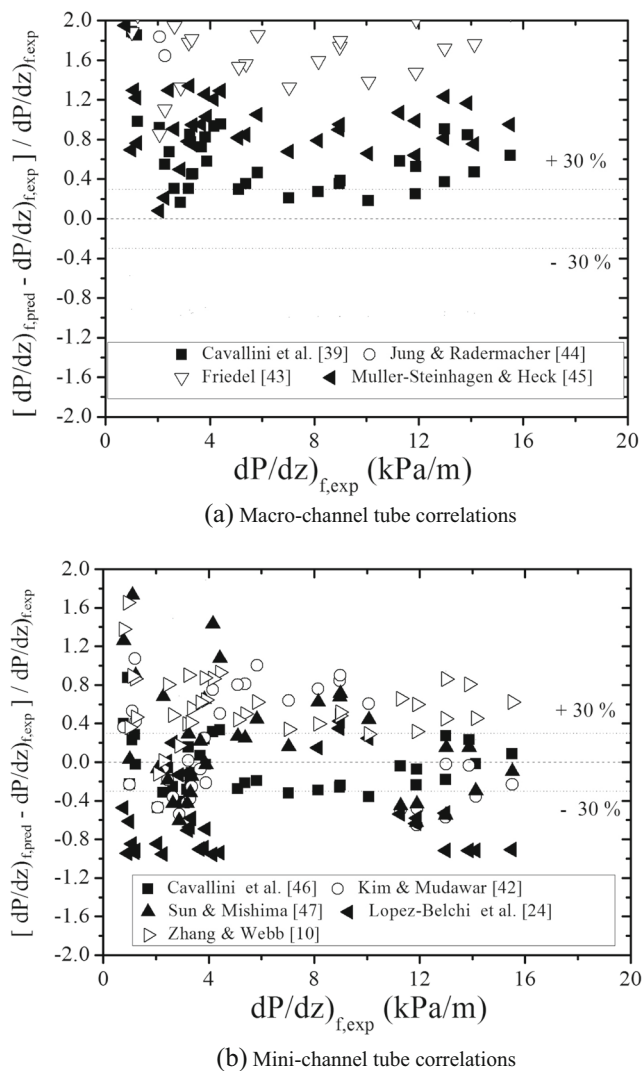


**Fig. 12** Present frictional pressure gradients compared macro- and mini-channel tube correlations

## 5 Conclusions

R-410A condensation tests were conducted in four different smooth multi-port tubes having a range of hydraulic diameter ( $0.78 \leq D_h \leq 0.95$  mm). The test range covered the mass flux from 100 to 400 kg/m<sup>2</sup> s and the heat flux was fixed at 3 kW/m<sup>2</sup>, which are typical operating conditions of a residential air conditioner. The saturation temperature was 45° C. Listed below are major findings.

- 1) Both the heat transfer coefficient and the pressure drop increased as the hydraulic diameter decreased.
- 2) The effect of hydraulic diameter on condensation heat transfer was much larger than the predictions of existing correlations for the range of investigation.
- 3) Both the macro-channel tube correlation [39] and the mini-channel correlation [6] reasonably predicted the heat transfer coefficient.

- 4) Only mini-channel correlation, e. g. Cavallini et al. [46], adequately predicted the pressure drop. Macro-channel correlations highly overpredicted the data.
- 5) Number of channels and channel aspect ratio may also be responsible for the difference in the heat transfer coefficient of the present study in addition to the hydraulic diameter.

**Acknowledgements** This work was supported by Incheon National University Research Grant in 2015.

## References

1. Webb RL, Kim N-H (2005) Principles of enhanced heat transfer, 2nd edn. Taylor and Francis Pub, Milton Park
2. Yang CY, Webb RL (1996) Condensation of R-12 in small hydraulic diameter extruded aluminum tubes with and without micro-fins. *Int J Heat Mass Trans* 39(4):791–800
3. Webb RL, Yang CY (1995) A comparison of R-12 and R-134a condensation inside small extruded aluminum plain and micro-fin tubes. *IMEchE C4961053195:77–86*
4. Yang CY, Webb RL (1996) Frictional pressure drop of R-12 in small hydraulic diameter extruded aluminum tubes with and without micro-fins. *Int J Heat Mass Trans* 39(4):801–809
5. Chang YP, Tsai R, Hwang JW (1997) Condensing heat transfer characteristics of aluminum flat tube. *Applied Therm Eng* 17(11):1055–1065
6. Wang W-WW, Radcliff TD, Christensen RN (2002) A condensation heat transfer correlation for millimeter-scale tubing with flow regime transition. *Exp Thermal Fluid Sci* 26:473–485
7. Zhang M, Webb RL (2001) Correlation of two-phase friction for refrigerants in small-diameter tubes. *Exp Thermal Fluid Sci* 25:131–139
8. Kim NH, Cho JP, Youn B (2003) Condensation of R-22 and R-410A in flat aluminum extruded tubes. *Int J Refrig* 26:830–839
9. Webb RL, Ermis K (2001) Effect of hydraulic diameter on condensation of R-134A in flat, extruded aluminum tubes. *J Enhanced Heat Trans* 8:77–90
10. Koyama S, Kuwahara K, Nakashita K, Yamamoto K (2003) An experimental study on condensation of R134a in a multi-port extruded tube. *Int J Refrig* 24:425–432
11. Cavallini A, Del Col D, Doretti L, Matkovic M, Rossetto L, Zilio C (2005) Condensation heat transfer and pressure gradient inside multiport minichannels. *Heat Trans Eng* 26(3):45–55
12. Bandhauer TM, Agarwal A, Garimella S (2006) Measurement and modeling of condensation heat transfer coefficients in circular microchannels. *J Heat Transf* 128:1050–1059
13. Agarwal A, Bandhauer TM, Garimella S (2010) Measurement and modeling of condensation heat transfer in non-circular microchannels. *Int J Refrig* 33:1169–1179
14. Park JE, Vakili-Farahani F, Consilini L, Thome JR (2011) Experimental study on condensation heat transfer in vertical minichannels for new refrigerant R1234ze(E) versus R134a and R236fa. *Exp Thermal Fluid Sci* 35:442–454
15. Sakamatapan K, Kaew-On J, Dalkilic AS, Mahian O, Wongwises S (2013) Condensation heat transfer characteristics of R-134a flowing inside the multiport channels. *Int J Heat Mass Trans* 64:976–985
16. Illan-Gomez F, Lopez-Belchi A, Garcia-Cascales JR, Vera-Garcia F (2015) Experimental two-phase heat transfer coefficient and friction pressure drop inside mini-channels during condensation with R1234yf and R134a. *Int J Refrig* 51:12–23
17. Lopez-Belchi A, Illan-Gomez F, Garcia-Cascales JR, Vera-Garcia F (2015) Heat transfer coefficient during condensation inside a

- minichannel multiport tube with R32 and R410A as working fluids. *Sci Tech Built Env* 21:535–544
18. Park CY, Hrnjak PS (2009) CO<sub>2</sub> Flow condensation heat transfer and pressure drop in multiport microchannels at low temperatures. *Int J Refrig* 32:1129–1139
  19. Heo J, Park H, Yun R (2013) Condensation heat transfer and pressure drop characteristics of CO<sub>2</sub> in a microchannel. *Int J Refrig* 36:1657–1668
  20. Fernando P, Palm B, Ameel T, Lundquist P, Grandy E (2008) A minichannel aluminum tube heat exchanger - part III: condenser performance with propane. *Int J Refrig* 31:696–708
  21. Akers WW, Deans HA, Crosser OK (1959) Condensation heat transfer within horizontal tubes. *Chem Eng Progress Symp Series* 55(29):171–176
  22. Shah MM (1979) A general correlation for heat transfer during film condensation in tubes. *Int J Heat Mass Trans* 22(4):547–556
  23. Yang CY, Webb RL (1997) A predictive model for condensation in small hydraulic diameter tubes having axial micro-fins. *J Heat Trans* 119:776–782
  24. Moser K, Webb RL, Na B (1998) A new equivalent Reynolds number model for condensation in smooth tubes. *J Heat Trans* 120:410–417
  25. Haraguchi H, Koyama S, Fujii T (1994) Condensation of refrigerant HCFC22, HFC134a and HCFC123 in a horizontal smooth tube (2nd report, proposal of empirical expressions for the local heat transfer coefficient). *Trans JSME (B)* 60(574):245–252 (in Japanese)
  26. Mishima K, Hibiki T (1996) Some characteristics of air-water flow in small diameter vertical tubes. *Int J Multiphase Flow* 22:703–712
  27. Webb RL, Zhang M, Narayanamurthy R (1998) Condensation heat transfer in small diameter tubes. In *Proc 11th IHTC* 6:403–408
  28. Yun JH, Jeong JW (2016) A review of prediction methods for two-phase pressure loss in mini/micro channels. *Int J Air-Cond Refrig* 24(1):1630002
  29. Kim NH (2015) Condensation and evaporation tests of newly developed microfin tubes. Internal Report to LG Electronics
  30. Kim NH, Lee EJ, Byun HW (2014) Condensation heat transfer and pressure drop in flattened smooth tubes having different aspect ratios. *Exp Thermal Fluid Sci* 46:245–253
  31. Wilson EE (1915) A basis for rational design of heat transfer apparatus. *Trans ASME* 37:47–70
  32. Collier JG, Thome JR (1994) Convective boiling and condensation, 3rd edn. Oxford University Press, Oxford
  33. Zivi SM (1964) Estimation of steady state steam void fraction by means of principle of minimum entropy production. *J Heat Trans* 86:237–252
  34. Klein SJ, McClintock FA (1953) The description of uncertainties in single sample experiments. *Mech Eng* 75:3–9
  35. Garimella S (2010) Condensation flow mechanisms in microchannels: basis for pressure drop and heat transfer models. *Heat Trans Eng* 25(3):104–116
  36. Lopez-Belchi A, Vera-Garcia F, Garcia-Cascales JR (2015) Non-uniform condensation of refrigerant R-134a in multi-channel multiport tubes: two-phase pressure drop and heat transfer coefficient. *J Enhanced Heat Trans* 22(5):391–416
  37. Shah MM (2009) An improved and extended general correlation for heat transfer during condensation in plain tubes. *Int J HVAC & R Research* 15(5):889–913
  38. Dobson MK, Chato JC (1998) Condensation in smooth horizontal tubes. *J Heat Trans* 120:193–213
  39. Cavallini A, Censi G, Del Col D, Doretti L, Longo GA, Rossetto L (2002) Condensation of halogenated refrigerants inside smooth tubes. *Int J HVAC & R. Research* 8(4):429–451
  40. Thome JR, El Hajal J, Cavallini A (2003) Condensation in horizontal tubes, Part2: new heat transfer model based on flow regimes. *Int J Heat Mass Trans* 46:3365–3387
  41. Shah MM (2016) A correlation for heat transfer during condensation in mini/micro channels. *Int J Refrig* 64:187–202
  42. Kim SM, Mudawar I (2012) Flow condensation in parallel microchannels - part 2: heat transfer results and correlation technique. *Int J Heat Mass Trans* 55:984–994
  43. Jung D, Radermacher R (1989) Prediction of pressure drop during horizontal annular flow boiling of pure and mixed refrigerants. *Int J Heat Mass Trans* 32(12):2435–2446
  44. Friedel L (1979) Improved friction pressure drop correlations for horizontal and vertical two phase pipe flow. Paper E2, European Two Phase Flow Group Meeting, Ispra
  45. Muller-Steinhagen H, Heck K (1986) A simple friction pressure drop correlation for two-phase flow in pipes. *Chem Eng Process* 20:297–308
  46. Cavallini A, Del Col D, Matkovic M, Rossetto L (2009) Frictional pressure drop during vapor-liquid flow in minichannels: modeling and experimental evaluation. *Int J Heat Fluid Flow* 30:131–191
  47. Sun L, Mishima K (2009) Evaluation analysis of prediction methods for two-phase flow pressure drop in mini-channels. *Int J Multiphase Flow* 35:47–54